Arch. Metall. Mater. **70** (2025), 2, 937-942

DOI: https://doi.org/10.24425/amm.2025.153497

M. CZERNY[1], A. SZEWCZYK[1], P. PETRZAK[1], J. SKIBA[2], N. SCHELL[3], R. CHULIST[1*]

EVOLUTION OF MICROSTRUCTURE AND CRYSTALLOGRAPHIC TEXTURE IN SEVERELY DEFORMED FeCoNiAlTi MULTICOMPONENT ALLOY

The evolution of microstructure, texture, phase composition, and dislocation density distribution in Fe-based shape memory alloys processed by high-pressure torsion (HPT) at room temperature was investigated using synchrotron radiation and electron backscatter diffraction. The initial material was a hydrostatically extruded sample that underwent additional heat treatment. Before HPT deformation, the disks were heat treated at 1200°C for 5 mins. to relieve the stresses. The starting Fe-based material was characterized by a strong fibre <111> texture and coarse columnar grains with an average size of approximately 200 μm. The HPT process alters the initial <111> strong fibre texture to a typical shear texture with dominating B, $\overline{B}$, A_1^* and A_2^* components. As deformation proceeds marginal precipitation of β phase occurs. The precipitation process seems to be related to the shear magnitude, as the volume fraction of β phase increased linearly with shear. Furthermore, the precipitates produced by HPT form a typical texture for *bcc* metals with F and J1 components.

Keywords: Texture; HPT; synchrotron diffraction; multicomponent alloy

1. Introduction

Iron-based multicomponent alloys are a class of materials known for their remarkable ability to superelastic effect, high strength and excellent soft magnetic properties [1-10]. Unlike traditional alloys, the Fe-based alloys exhibit a superelastic effect near room temperature or even at lower temperatures, making them highly valuable for a wide range of engineering applications, including actuators and biomedical devices [11-21]. Concurrently, due to their complex chemical composition, Fe-based multicomponent alloys allow for easy control of microstructural features through massive solid solution formation, phase stabilization, and precipitation hardening. In this context, two types of precipitates can evolve within the solid matrix. The first one is the coherent γ' phase which is of great interest due to its impact on superelastic properties [11,16]. This effect is strongly dependent on the precipitation hardening conditions (temperature, time, initial state of the material) that strengthen the matrix and provide stress concentrators that stimulate stress-induced martensitic transformation [22-28]. The second precipitate is the incoherent B2-based β phase, which significantly affects both the magnetic and mechanical properties. In light of these findings, precipitation hardening is a key factor in tuning the mechanical and magnetic properties of Fe-based multicomponent alloys. Therefore, in this paper, the main focus is to study the effect of severe plastic deformation on the precipitation process.

Another important factor is crystallographic texture. Superelastic strain, a unique property of shape memory alloys (SMAs), is activated along specific crystallographic planes and directions. This is also true for magnetic and mechanical properties, which are strongly anisotropic. Therefore, the texture is a crucial element that should be analyzed and optimized. For these reasons, Fe-based multicomponent alloys with a composition of Fe-28Ni-17Co-11.5Al-2.5Ti (in at.%, abbreviated NCAT) were subjected to hydrostatic extrusion (HSE), heat treatment, and finally high-pressure torsion (HPT). Deformation can lead to a preferred orientation, which can vary depending on the specific deformation process. In high-pressure torsion, simple shear is the dominant deformation mode and the magnitude of shear changes along the sample radius. This characteristic allows for a wide range of investigations using just one sample. Severe plastic deformation can also produce ultrafine-grained materials. Therefore, to explore the effect of HPT on microstructure, texture, phase composition, dislocation density, and microstrains, synchrotron

[1] INSTITUTE OF METALLURGY AND MATERIALS SCIENCE PAS, 30-059 KRAKOW, POLAND
[2] INSTITUTE OF HIGH PRESSURE PHYSICS OF THE POLISH ACADEMY OF SCIENCES,UNIPRESS, 29/37 SOKOLOWSKA STR., 01-142WARSAW, POLAND
[3] INSTITUTE OF MATERIALS PHYSICS, HELMHOLTZ-ZENTRUM HEREON, MAX-PLANCK-STRASSE 1, D-21502 GEESTHACHT, GERMANY

* Corresponding author: rchulist@agh.edu.pl

radiation and electron backscatter diffraction (EBSD) were used. Applying these techniques, the evolution of microstructure and texture was analyzed in relation to the deformation mode, heat treatment, and precipitation hardening.

2. Experimental

The initial material was cast in the shape of a cylinder of diameter 13 cm with Fe-28Ni-17Co- 1.5Al-2.5Ti composition. Secondly, the material was hydrostatically extruded at room temperature. After extrusion, the cross-section was reduced from 13 mm to 10 mm in one pass at room temperature. The material was extruded with pressures in the range 400-500 MPa. Prior to HPT deformation, the alloy was heat-treated at 1200°C for 5 minutes [1]. Three small disks, with a diameter of 10 mm and a height of 2 mm, were cut from the initial bar by spark erosion. The following coordinate system was applied so that the extrusion direction (ED) was parallel to the normal direction (|| HPT process). The disks were subsequently deformed at room temperature by HPT for 1, 2, and 5 rotations under a constant pressure of 2 GPa. In order to perform phase analyses, high-energy X-ray diffraction measurements were carried out using the HZG beamline (P07B) located at PETRA III with wavelength, $\lambda = 0.142342$ Å at DESY, Hamburg, Germany. In order to eliminate the texture effect and to obtain highly comparable results, all samples were rotated 180° about the ω angle during measurements (the so-called continuous mode) [29-31]. The crystallographic texture of all states was also measured using high-energy synchrotron radiation by a step size of 5°. For local texture and phase analyses, cuboid samples with dimensions of 2.0 mm × 2.0 mm × 13 mm were cut. The samples were transmitted with a beam size of 0.8×0.8 mm. The shear strain value given corresponds to the middle of the respective analyzed volume. Experimental pole figures were calculated using StressTexCalculator software [32], and the orientation distribution function (ODF) was obtained using LABOTEX software. The following pole figures were measured: {111}, {200}, {220} for the *fcc* matrix, and {110}, {200}, {211} for the β phase-type precipitates [33]. A typical monoclinic symmetry of simple shear, along with standard crystal and sample coordinate systems, was employed [34]. Texture images are represented by $\phi 2 = 0°$ and 45° ODF sections, which allow for easy detection and interpretation of all major texture components. To estimate the volume fraction of particular phases High Score Plus software was employed. The used parameters ensured good counting statistics with a typical value of goodness of fit parameter lower than 2 for all Rietveld quantifications. The microstrains were calculated using the following formula $\varepsilon = \beta\cos\theta/4$, where ε is a microstrain, β is the full-width at half maximum (FWHM). Dislocation density was estimated using $\delta = (K\lambda/\beta\cos\theta)2$ formula, where K is constant. [30,31]. All states were also investigated by FEI Quanta 3D FEG scanning electron microscope operated at 20 kV and equipped with EDAX OIM TSL EBSD collecting system to reveal the microstructure of the NCAT alloys.

3. Results and discussion

Fig. 1 represents the diffraction pattern for all the examined samples. As can be seen in the as extruded and annealed state solely the fcc matrix is present. The only difference lies in the position and broadening of diffraction peaks indicating a much higher dislocation density and internal stresses in the HSE sample. Annealing at 1200°C provides softening of the material relieving the stresses.

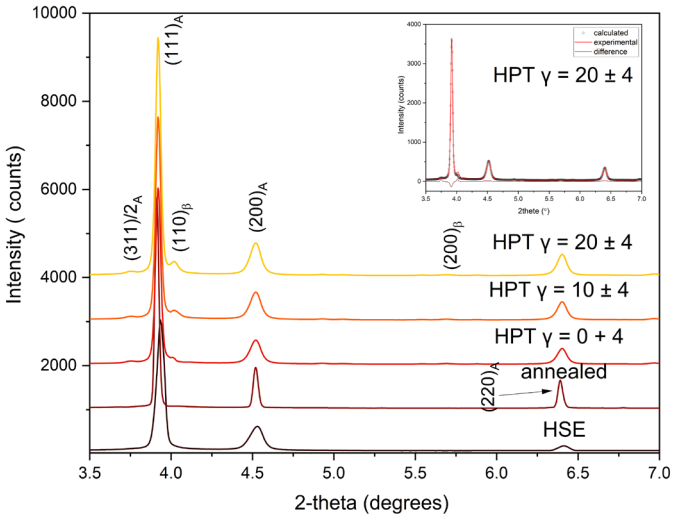

Fig. 1. Synchrotron diffraction pattern of differently deformed and annealed NCAT samples. (HSE – hydrostatic extrusion, HPT – high-pressure torsion). Inset demonstrates the Rietveld refinement for HPT deformed sample

It also changes the grain size as shown in Fig. 2 producing coarse equiaxed grains with an average size of around 200 µm. However, upon HPT deformation, high strains cause broadening of diffraction profiles indicating again a gradual increase in dislocation density as the shear magnitude increases. In addition, the β phase is recognized by a small intensity of (110) reflection. The volume fraction of the β phase maintains a higher value with increasing shear gradually reaching eventually 3.8% for $\gamma = 20$, Fig. 3b.

As can be seen in Fig. 2, HPT successfully refined the microstructure with an average size of about 5 µm and 1 µm for γ = 10 and 20, respectively. The size of the β precipitates is beyond the spatial resolution of EBSD (40 nm) being in the nanometer range. Shear deformation also changes the shape of austenitic grains from around equiaxed to ellipse shape with the long axis inclined toward the shear direction (SD). Using a diffraction pattern the dislocation density and microstrains were calculated. Fig. 3(a) reveals both parameters following the deformation path. After one pass of HSE the density of dislocation rises to 1.1×10^{15} m^{-2}. Heating at 1200°C causes a sudden drop in microstrains and dislocation density by an order of magnitude to about 0.001% and 1.0×10^{14} m^{-2}, respectively. Nevertheless, HPT process progressively increases both features reaching values of about 40% higher than for the HSE sample. Fig. 3(b) shows the

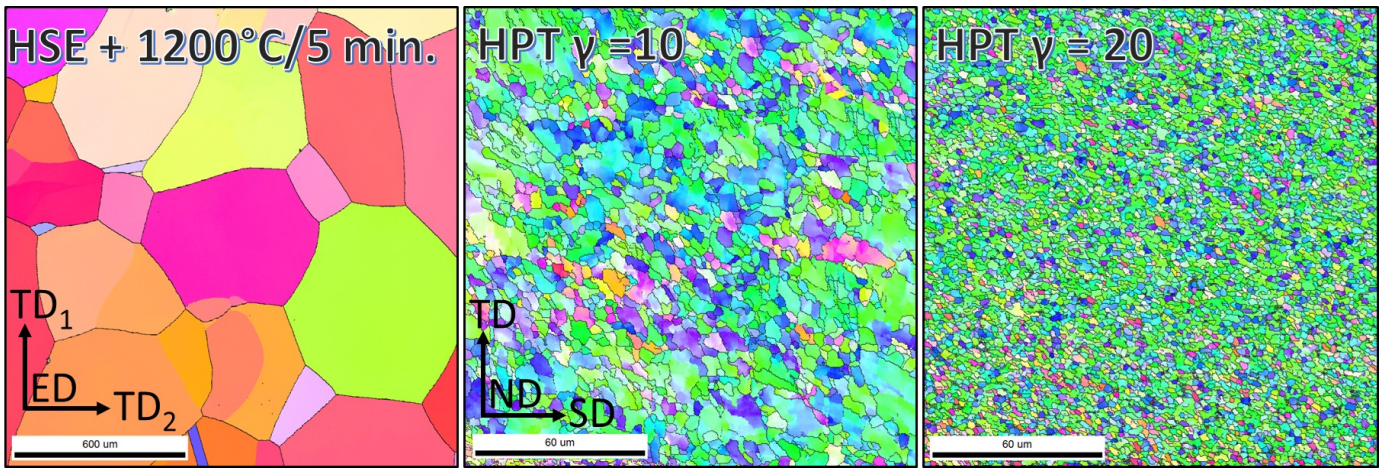

Fig. 2. EBSD maps of the initial material and subjected to HPT at a shear strain of about 10, and 20

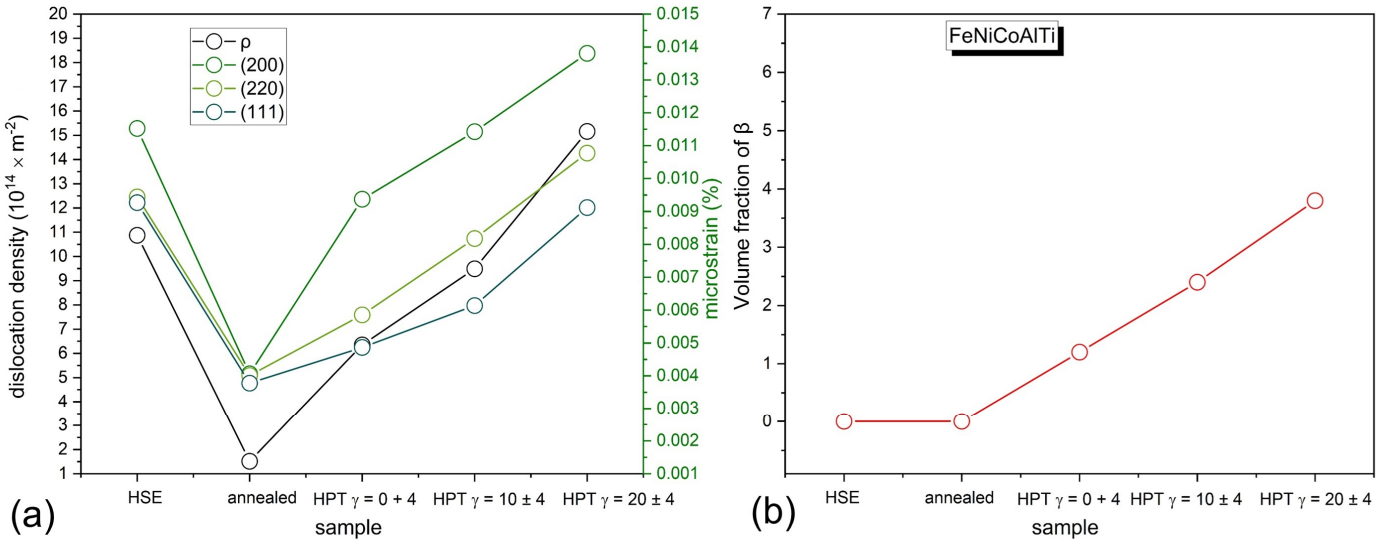

Fig. 3. (a) Microstrains and dislocation density calculated from high-energy X-ray diffraction patterns for all samples along with (b) volume fraction of the β phase

calculated by Rietveld refinement volume fraction of β phase. As can be seen, the amount of beta phase linearly increases with shear deformation and finally equals 3.8% for $\gamma = 20$. This clearly demonstrated that the β phase is generated by a shear-driven phase transition as there was no heat treatment applied after HPT. It is worth mentioning that compared to our previous study the quantity of the β phase is significantly reduced [35] reaching a very small value. Thus, HPT leads to a precipitation process promoting the NiAl-B2 (β) type intermetallic phase. However, the amount of NiAl-B2 is very small.

Fig. 4 shows the ODF sections at $\varphi 2 = 0°$ and 45° which clearly indicate that the initial texture of the HSE processed sample is characterised by a strong <111> fibre component. The <111> direction is predominantly aligned with the extrusion direction which means that this is also the rotation axis for HPT process. Anealing does not change the texture qualitatively since it remains strong <111>, however a new weak <100> fibre appears. The shear deformation of the matrix produces a typical shear texture for *fcc* metals. Mainly $B, \overline{B}, A_1^*$ and A_2^* components are detected [36]. The intensity of these components increases as the magnitude of shear increases. On the other hand, the texture of β *bcc*-based precipitates is characterized by F and J components [37]. Interestingly one of the J components and D components are missing which can point to some variant selections. It is also unexpected that the shear texture of precipitates is quite pronounced even though the volume fraction of them is very low.

4. Conclusions

The following conclusions can be drawn based on the experimental results:

1. HSE produces a strong <111> fibre texture of the fcc phase with no trace of bcc precipitates.
2. After annealing, no significant change in the texture is observed, except for stress relief and grain growth.
3. HPT performed at room temperature leads to marginal precipitation of B2 phase.

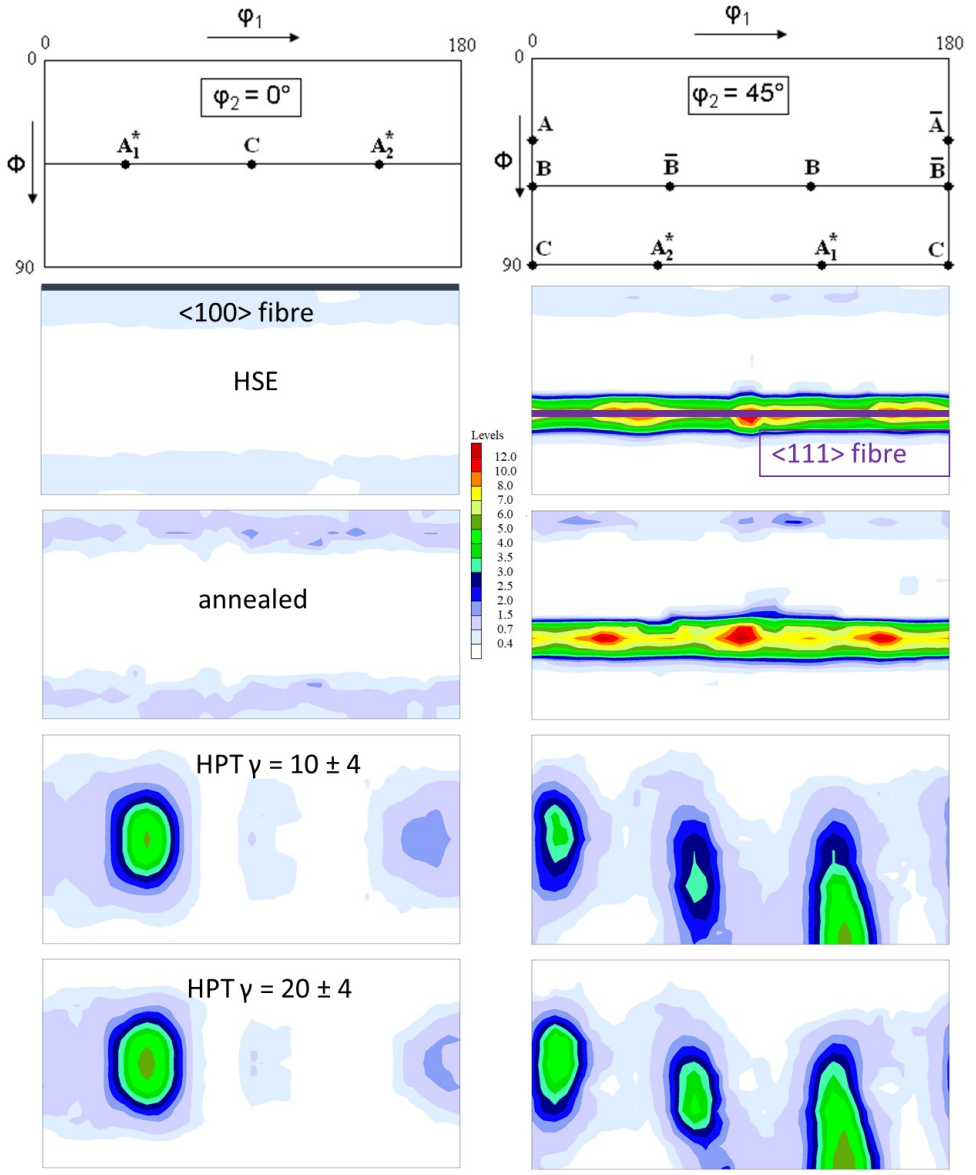

Fig. 4. ODF sections at $\varphi 2 = 0°$ and 45 of the initial HSE sample, annealed and after HPT at a shear strain of 10 and 20 for the matrix phase. Key figures give the ideal components of simple shear of *fcc* metals. Intensities are provided in multiples of random distribution (mrd)

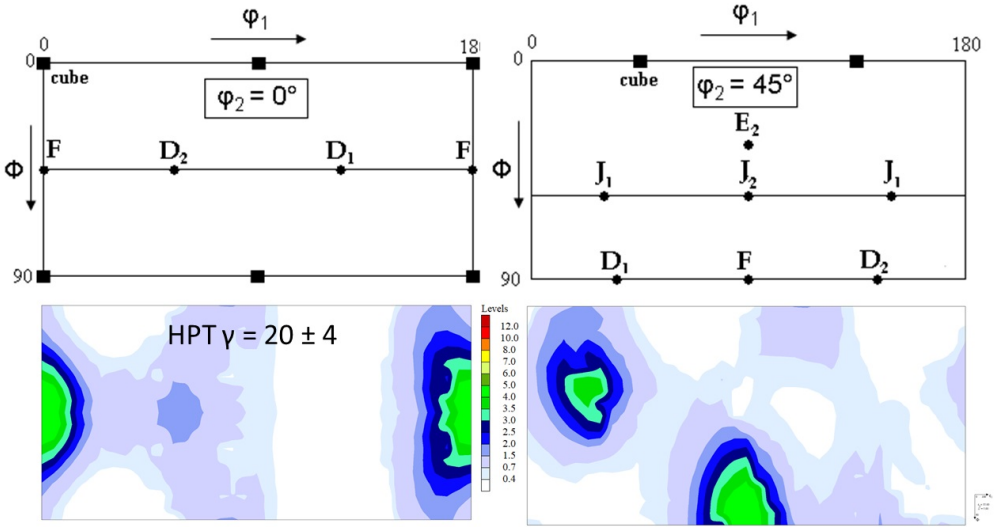

Fig. 5. ODF sections at $\varphi 2 = 0°$ and 45 of the sample subjected to HPT at a shear strain of 20 for β phase. Key figures give the ideal components of simple shear of *bcc* metals

4. The texture of Fe-based alloys subjected to the HPT process is characterized by strong B, $\overline{B}$, A_1^* and A_2^* omponents while F and J shear components of *bcc* metals are found.
5. No D and only one J shear component after application of high shear is found in the bcc phase indicating strong variant selections.

Acknowledgment

The financial support of the National Science Centre of Poland through project 2020/37/N/ST5/03134 is acknowledged.

REFERENCES

[1] Y. Tanaka, Y. Himuro, R. Kainuma, Y. Sutou, T. Omori, K. Ishida, Science **327**, 1488 (2010).

[2] T. Omori, K. Ando, M. Okano, X. Xu, Y. Tanaka I. Ohnuma, R. Kainuma, K. Ishida, Science **333**, 68 (2011).

[3] Y.I. Chumlyakov, I. Kireeva, E. Panchenko, I. Karaman, H.J. Maier, E. Timofeeva, J. Alloys Comp. **577**, S393-S398 (2013).

[4] Y.I. Chumlyakov, I. Kireeva, I. Kretinina, I.V. Kuts, O.A. Kejnih, K.S. Kirillov, V.A. Karaman, I. Maier, H.J. Karaka, Thermoelastic martensitic transformations into new high-strength FeNiCoAlX (X = Ta, Ti, Nb, B) single crystals. Abstract Book, ICOMAT, Bilbao Spain (2014).

[5] E.P. George, D. Raabe , R.O. Ritchie, Nat. Rev. Mater. **4**, 515-534. (2019).

[6] L. Han, F. Maccari, I.R. Souza Filho, N.J. Peter, Y. Wei, B. Gault, O. Gutfleisch, Z. Li, D. Raabe, Nature **608**, 310-316 (2022).

[7] Y. Ma, Q. Wang, X. Zhou, J. Hao, B. Gault, Q. Zhang, Ch. Dong, T.G. Nieh, Adv. Mater. **33**, 2006723 (2021).

[8] L. Han, Z. Rao, I.R. Souza Filho, F. Maccari, Y. Wei, G. Wu, A. Ahmadian, X. Zhou, O. Gutfleisch, D. Ponge, D. Raabe, Z. Li, Adv. Mater. **33**, 2102139 (2021).

[9] E. Hornbogen, W. Meyer, Acta Metall. **15**, 584 (1967).

[10] T. Maki, in: K. Otsuka, C.W. Wayman (Eds.), Shape Memory Materials, Cambridge.

[11] H. Sehitoglu, I. Karaman, X.Y. Zhang, Y. Chumlyakov, H.J. Maier, Scripta Mater. 44.

[12] Y. Tanaka, Y. Himuro, R. Kainuma, Y. Sutou, T. Omori, K. Ishida, Science **327**, 1488 (2010).

[13] I.V. Kireeva, Y.I. Chumlyakov, V.A. Kirillov, I. Karaman, E. Cesari, Tech. Phys. Lett. **37**, 86 (2011).

[14] J. Ma, B. Kockar, A. Evirgen, I. Karaman, Z.P. Luo, Y. Chumlyakov, Acta Mater. **60**, 2186 (2012).

[15] Y.I. Chumlyakov, I.V. Kireeva, E.Y. Panchenko, V.A. Kirillov, E.E. Timofeeva, I.V. Kretinina, Y.N. Danil'son, I. Karaman, H. Maier, E. Cesari, Russ. Phys. J. **54**, 937 (2012).

[16] J. Ma, B.C. Hornbuckle, I. Karaman, G.B. Thompson, Z.P. Luo, Y.I. Chumlyakov, Acta. Mater. **61**, 3445 (2013).

[17] D. Lee, T. Omori, R. Kainuma, J. Alloys and Compd. **617**, 120 (2014).

[18] L.W. Tseng, Ji Ma, I. Karaman, S.J. Wang, Y.I. Chumlyakov, Scr. Mater. **101**, 1 (2015).

[19] Y.I. Chumlyakov, I.V. Kireeva, O.A. Kutz H.E. Karaca, I. Karaman, Scripta Mater. **119**, 43-46 (2016).

[20] P. Krooß, M.J. Holzweissig, T. Niendorf, C. Somsen, M. Schaper, Y.I. Chumlyakov, H.J. Maier, Scripta Mater. **81**, 28-31 (2014).

[21] Y. Tanaka, R. Kainuma, T. Omori ,K. Ishida, Mat. Today Proc. **2S**, S485-492 (2015).

[22] H. Fu, H. Zhao, Y. Zhang, J. Xie, Enhancement of Superelasticity in Fe-Ni-Co-Based Shape Memory Alloys by Microstructure and Texture Control. Procedia Engineering **207**, 1505-1510 (2017). DOI: https://doi.org/10.1016/j.proeng.2017.10.1084

[23] H. Fu, W. Li, S. Song, Y. Jiang, J. Xie, Effects of grain orientation and precipitates on the superelasticity in directionally solidified FeNiCoAlTaB shape memory alloy. Journal of Alloys and Compounds **684**, 556-563 (2016). DOI: https://doi.org/10.1016/j.jallcom.2016.05.209

[24] J.H. Yang, H. Chen, C.M. Wayman, Development of Fe-based shape memory alloys associated with face-centered cubic-hexagonal close-packed martensitic transformations: Part I. shape memory behavior. Metallurgical Transactions A **23** (5), 1431-1437 (1992). DOI: https://doi.org/10.1007/bf02647326

[25] J.H. Yang, H. Chen, C.M. Wayman, Development of Fe-based shape memory alloys associated with face-centered cubic-hexagonal close-packed martensitic transformations: Part II. transformation behavior. Metallurgical Transactions A **23** (5), 1439-1444 (1992). DOI: https://doi.org/10.1007/bf02647327

[26] J.H. Yang, C.M. Wayman, Development of Fe-based shape memory alloys associated with face-centered cubic-hexagonal close-packed martensitic transformations: Part III. microstructures. Metallurgical Transactions A **23** (5), 1445-1454 (1992).

[27] J. Mohd Jani, M. Leary, A. Subic, M.A. Gibson, A review of shape memory alloy research, applications and opportunities. Materials & Design (1980-2015), **56**, 1078-1113 (2014). DOI: https://doi.org/10.1016/j.matdes.2013.11.084

[28] F. Jemal, T. Bouraoui, T. Ben Zineb, E. Patoor, C. Bradaï, Modelling of martensitic transformation and plastic slip effects on the thermo-mechanical behaviour of Fe-based shape memory alloys. Mechanics of Materials **41** (7), 849-856 (2009). DOI: https://doi.org/10.1016/j.mechmat.2008.11.007

[29] R. Chulist, A. Wójcik, A. Sozinov, T. Tokarski, M. Faryna, N. Schell, W. Skrotzki, B. Li, H. Sehitoglu, X. Li, W. Maziarz, Adaptive Phase or Variant Formation at the Austenite/Twinned Martensite Interface in Modulated Ni–Mn–Ga Martensite. Advanced Fuctional Materials **34**, 2307322 (2024).

[30] A. Wójcik, R. Chulist, A. Szewczyk, B. Morończyk, Ł. Żrodowski, R. Wróblewski, M. Kowalczyk, A. Kolano-Burian, P. Zackiewicz, N. Schell, W. Maziarz, Microstructure and texture control of Ni-Mn-Ga magnetic shape memory alloys manufactured by laser powder bed fusion. Additive Manufacturing **86**, 104225 (2024).

[31] A. Wójcik, R. Chulist, P. Czaja, M. Kowalczyk, P. Zackiewicz, N. Schell, W. Maziarz, Evolution of microstructure and crystallographic texture of Ni-Mn-Ga melt-spun ribbons exhibiting 1.15% magnetic field-induced strain. Acta Materialia **219** (2021).

[32] C. Randau, U. Garbe, H-G. Brokmeier, J. Appl. Crystallogr. **44**, 641-646 (2011).
[33] K. Pawlik, P. Ozga, Gottinger Arb. Geol. Palaont. **SB4**, 146 (1999).
[34] L.S. Toth, A. Molinari, Acta Metall. Mater. **42**, 2459 (1994).
[35] R. Chulist, M. Czerny, A. Panigrahi, M. Zehetbauer N. Schell, W. Skrotzki, Texture and microstructure of HPT-processed Fe-based shape memory alloys. IOP Conference Series: Mater. Sci. Eng. **375** (1), 01 (2006).
[36] R. Chulist, W. Skrotzki, C.-G. Oertel, A.Bohm, H.-G. Brokmeier, T. Lippmann, Int. J. Mater. Res. **103**, 575 (2012).
[37] H.J. Bunge, Texture Analysis in Materials Science, Mathematical Methods, Culliver Verlag, Goettingen 1993.